The dipolar fluctuation spectrum and the shape of the wings of nuclear magnetic resonance absorption spectra in solids

1990 J. Phys.: Condens. Matter 2 10131

(http://iopscience.iop.org/0953-8984/2/50/017)

J. Phys.: Condens. Matter 2 (1990) 10131–10145. Printed in the UK

The dipolar fluctuation spectrum and the shape of the wings of nuclear magnetic resonance absorption spectra in solids

A A Lundin, A V Makarenko and V E Zobov†
N N Semenov Institute of Chemical Physics, Academy of Sciences of the USSR, Kosygina 4, Moscow, 117977 GSP-1, USSR

Received 28 February 1990, in final form 23 August 1990

Abstract. A theoretical approach providing the shape of the spectrum of dipolar fluctuations (Fourier transform of the longitudinal component of magnetization) and shape of the wings of NMR absorption in condensed matter has been elaborated. It is shown that the spectral contours are exponentials with the same decay constant. The results obtained explain for the first time the known experimental data and establish a connection between two groups of different experiments. The theoretical prediction is in good agreement with experimental results.

1. Introduction

In 1969, McArthur *et al* [1] experimentally observed for the first time the exponential dependence of the rate of cross relaxation accompanying double resonance as a function of detuning.

Thus, it was found that Fourier transform of the time correlation function (TCF) of the longitudinal (with respect to an external magnetic field) component of magnetization considered for not too long times was an exponential function of frequency. The detected spectrum was called a spectrum of dipolar fluctuations (SDF). This result was quite unexpected when considered against the background of the widely accepted concept that the absolute majority of TCFs derived by magnetic resonance techniques were of Gaussian or Lorentzian type. Subsequently, the results of [1] have often been confirmed experimentally at various objects (see, e.g., [2]) and by different techniques [3, 4].

Up to now the above results have not been explained and, as was pointed out in [5], the sense of phenomenological approximations for memory functions [6] given in [7] to describe the results of [1] is vague. This fact was also noted in [7]. For application to the problem of the shape of the wings of NMR absorption the analogous procedure results in a Gaussian shape [8]. As will be shown below this is not the case (see also [9]). Thus, exponential frequency asymptotics of TCF spectra observed in NMR have neither a qualitative nor a quantitative description.

† Permanent address: L V Kirensky Institute of Physics, Siberian Branch of the Academy of Sciences of the USSR, Academgorodok, Krasnoyarsk, 660036, USSR.

0953-8984/90/5010131 + 15 $03.50

In the present communication a description of the SDF and the shape of the wings of the NMR line is given in terms of the theory developed. It is shown that they are exponential functions having the same decrement constants. The results of calculations are in qualitative and quantitative agreement with experimental results [1, 10].

2. Basic equations

It is known [11] that in non-metallic diamagnetic solids the broadening of spectra stems from a secular part of the dipole–dipole interaction between nuclear spins:

$$H = \sum_{i>j} b_{ij} S_{z_i} S_{z_j} + \sum_{i>j} a_{ij} (S_i^+ S_j^- + S_i^- S_j^+) = H_{zz} + H_{\mathrm{ff}} \tag{1}$$

$a_{ij} = -\frac{1}{4} b_{ij}$ (here we use the same notation as in [11]).

As known (see, e.g., [12, 13] the TCF under the most general assumptions satisfies the following integral–differential equation:

$$\frac{\mathrm{d}F}{\mathrm{d}t} = -\int_0^t M(t-t')F(t')\,\mathrm{d}t. \tag{2}$$

Thus, the equations for application to high-temperature spin systems were obtained in [13–15] and a constructive procedure was proposed in [14] to determine the memory function $M(t)$ for the system having a large number of near neighbours. This idea was realized in [15] during the calculation of several correlation functions in spin systems described by the above Hamiltonian (1). Consequently, for the autocorrelation functions of longitudinal $\Gamma_A^z(t)$ and lateral $\Gamma_A(t)$ (with respect to an outer magnetic field) components of a separate spin the equations strictly analogous to equation (2) are valid [13–15]. Equation (2) also holds for a correlation function of a transverse component of entire spin $\Gamma(t)$ including cross TCF terms between all different spins. $R_A^{(z)}(t)$, $R_A(t)$ and $R(t)$ are kernels (memory functions) of the appropriate equations. Our TCFs have an ordinary form [11, 13–16] (e.g. $\Gamma_A^z(t) = (1/A_1)\,\mathrm{Sp}[\exp(\mathrm{i}Ht)\,S_{z_i}\exp(-\mathrm{i}Ht)\,S_{z_i}]$ and are normalized to unity at $t = 0$.

The memory functions (irreducible operators) in equation (1) are series with respect to irreducible diagrams [14, 15] (see the appendix; see also the review in [16]). The algorithm developed in [14] was applied to computation of the TCF for paramagnets with an isotropic Heisenberg interaction. The spherical symmetry of the problem [14] resulted in a choice of correlation functions of a free particle (unperturbed Green functions) of the same form for x, y and z components: $G_0(t) = 1$. At the same time, application of the analogous choice of unperturbed functions (1 for transverse and longitudinal components) to the computation of TCF having an anisotropic interaction (1) resulted in a not very successful description of even the central part (and certainly not of the wings) of the NMR spectrum using the non-linear equation (2). We should remark that the difference between the unperturbed Green functions of the longitudinal and transverse components has a significant character since it reflects the fundamental fact that TCFs of longitudinal spin components decay relatively slowly with respect to the TCFs of transverse components [1, 6] owing to the symmetry of the Hamiltonian (1).

So, as a first stage, we explicitly summed the inputs from the H_{zz} interaction of the Hamiltonian (1) in a series of $\Gamma_A(t)$ which in fact made it possible to form a new unperturbed Green function for a transverse component (see the appendix and also [17]).

In the remaining part of the series for $\Gamma_A(t)$ we can sum the diagrams by a technique proposed in [14]. Thus, we obtain for $\Gamma_A(t)$ the following:

$$\Gamma_A(t) = G_0(t) - \int_0^t G_0(t-t') \int_0^{t'} K_A(t'-t'')\Gamma_A(t'')\,dt'\,dt'' \qquad (3)$$
$$K_A(t) = R_A(t) - Q(t).$$

Diagram series for $R_A(t)$ and $Q(t)$ are described in the appendix (equations (A5), (A6), (A7*a*) and (A11)). We should emphasize that equation (3) can be obtained from equation (2) on a formal basis without any detailing of functions $R_A(t)$ and $Q(t)$. In the same manner we obtain for $\Gamma(t)$ the following:

$$\Gamma(t) = G_0(t) - \int_0^t G_0(t-t') \int_0^{t'} K(t'-t'')\Gamma(t'')\,dt'\,dt'' \qquad (4)$$
$$K(t) = R(t) - Q(t)$$

where $R(t)$ is defined by equation (A7*a*). Although equations (3) and (4), similarly to the initial equation (2), are exact when the whole series is retained for the memory function within the limit of a large amount of neighbours ($Z \to \infty$) and high temperatures ($T \to \infty$), a first-term approximation of the irreducible operators $K(t)$ corresponding to diagrams with two vertices gives a precision sufficient to describe the experimental results [1, 5, 10]. This is the consequence of the initial partial summation of a series for $G_0(t)$. All correction terms for diagrams with two vertices appearing in the next order and containing four vertices were calculated. The expressions derived are given in the appendix.

Thus, substitution of appropriate expressions for memory functions in the lowest-order approximations (equations (A6), (A7) and (A12) in equations (2), (3) and (4), respectively) yields

$$G_0(t) = \exp\left(-\int_0^t \int_0^{t'} \Gamma_A^z(t'')\,dt'\,dt''\right) \qquad (5)$$

$$\Gamma_A^z(t) = 1 - \varepsilon_1 \int_0^t \int_0^{t'} \Gamma_A^2(t'-t'')\Gamma_A^z(t'')\,dt'\,dt'' \qquad (6)$$

$$\Gamma_A(t) = G_0(t) - \varepsilon_2 \int_0^t G_0(t-t') \int_0^{t'} \Gamma_A(t'-t'')\Gamma_A^z(t'-t'')\Gamma_A(t'')\,dt'\,dt'' \qquad (7)$$

$$\Gamma(t) = G_0(t) - \varepsilon_3 \int_0^t G_0(t-t') \int_0^{t'} \Gamma_A(t'-t'')\Gamma_A^z(t'-t'')\Gamma(t'')\,dt'\,dt''. \qquad (8)$$

The time is dimensionless in the system (5)–(8). The scale is defined by the value of $B = \sqrt{M_{2zz}}$, where M_{2zz} is an input into the second moment of NMR absorption spectrum of the Hamiltonian H_{zz} in (1). $\varepsilon_1 = \frac{1}{2}$; $\varepsilon_2 = \frac{1}{4}$, $\varepsilon_3 = \frac{5}{4}$. Finally we should point out that the system (5)–(8) was obtained in [17] by a somewhat different method from the present one.

Let us consider the possibility of linearizing the obtained system. First of all, we shall be interested in linearizing equations (7) and (8). Let us substitute for the function $\Gamma_A^z(t)$ the value unity in the kernels of equations (7) and (8). This is possible owing to a substantially shorter time scale of decay of the TCF $G_0(t)$, and of $\Gamma_A(t)$ with respect to $\Gamma_A^z(t)$ [1, 5, 18]. In agreement with the results of the above papers the decay time for

$\Gamma_A^z(t)$ is $T_2^* \simeq 3 \div 4T_2$, $T_2 = 1/\sqrt{M_2}$, where M_2 is the second moment of the NMR spectrum defined by the Hamiltonian (1). Further, let us substitute $\Gamma_A(t)$ by $G_0(t)$. Indeed, the second moment of these TCFs differs only in the factor $\frac{1}{16}M_2$; their shape, as a direct numerical experiment indicates [18], is approximately the same. This may be deduced directly from the system considered: equations (5) and (7) differ only in a small (proportional to $\frac{1}{4}$) term. Finally, since $T_2^* \simeq 3 \div 4T_2$, we may assume that fields created by the spins of a 'cell' [19, 20] have a quasi-static character. Because of this, $G_0(t) \simeq \exp(-B^2t^2/2)$.

Thus, we obtain the desired linearized form of equations (7) and (8). We get

$$\Gamma(t) = G_0(t) - \varepsilon_3 \int_0^t \mathrm{d}t' \, G_0(t-t') \int_0^{t'} \mathrm{d}t'' \, G_0(t'-t'')\Gamma(t'') \tag{9}$$

i.e. we obtain an equation coinciding with the major equation of [20]. The Fourier transform of a solution of equation (9) describes fairly well the major part of the NMR spectrum excluding the outside part of the wings. The linear equation (9) is in fact equation (8) with a memory function as the bare irreducible skeleton diagrams of the lowest order. Finally, after linearization, addition of the cross terms $\Gamma_{ij}^z(t)$, $i \neq j$, and appropriate easy calculations, equation (6) can be reduced at large times to an equation for spin diffusion [11].

A good description of the main features of free induction decay (FID) based upon (9) stems from the above procedure which makes it possible to take into account the non-equivalent character of unperturbed Green functions of transverse and longitudinal spin components.

However, the use of a system of non-linear equations is quite significant to describe the effects that we were dealing with. First, the system enables one to determine a direct relation of SDF to the shape of the NMR line and, second, linearization results in asymptotics of the type $\exp[-\alpha\omega \ln^{1/2}(\beta\omega)]$. The respective reasons will be analysed below.

3. The shape of the TCF spectra wings and analytical characteristics of the solutions

$G_0(t)$, $\Gamma_A^z(t)$ and $\Gamma_A(t)$ functions considered as functions of a complex variable have no singularities on the real axis. In fact on the real axis they describe the relaxation of the various components of magnetization to an equilibrium value varying from 1 (at $t = 0$) to 0 (when $|t| \to \infty$). At the same time, on extension to a plane of a complex variable τ, singularities may appear. This may be accompanied by two main possibilities.

(i) A singularity arises at an infinitely distant point.
(ii) A singularity arises at a final distance at a point τ_0.

A singularity in a complex plane strictly involves an exponential decrease in the distant Fourier components of the spectrum [21]:

$$f_\omega = \int_{-\infty}^{\infty} f(x) \exp(\mathrm{i}\omega x) \, \mathrm{d}x \sim \exp(-\omega x_1) \tag{10}$$

the approximation holding for $\omega x \gg 1$, where x_1 is the distance from a real axis to the nearest singularity in the complex plane. The relationship is independent of the type of isolated singularity (pole or branching point) [21]. In both cases, the asymptotics are

exponential. Only the appearance of singularities on a real axis, transforming the decay into oscillations, is critical with respect to exponential asymptotics.

The TCF of interest in (5)–(7) may be expanded into the series

$$G_0(t) = \sum_{n=0}^{\infty} (\mathrm{i})^{2n} \frac{G_{2n}}{(2n)!} t^{2n} \tag{11}$$

$$\Gamma_A(t) = \sum_{n=0}^{\infty} (\mathrm{i})^{2n} \frac{X_{2n}}{(2n)!} t^{2n} \tag{12}$$

$$\Gamma_A^z(t) = \sum_{n=0}^{\infty} (\mathrm{i})^{2n} \frac{Z_{2n}}{(2n)!} t^{2n}. \tag{13}$$

G_{2n}, X_{2n} and Z_{2n} are the moments of corresponding functions [11]. The radius of convergence of the series may be determined according to D'Alamber's formula:

$$\tau_0 = \sqrt{\lim_{n\to\infty} |a_{n-1}/a_n|} = \sqrt{\lim_{n\to\infty} [(M_{2n-2}/M_{2n})(2n-1)2n]}. \tag{13a}$$

Thus, the setting of moments enables one to determine the position of singularities. The higher the order of a known moment, the more precisely is a singularity localized. The substitution of expansion (11)–(13) into the system (5)–(7) and the equating of respective coefficients results in recurrence relations for moments:

$$G_{2n+2} = \sum_{m=0}^{n} G_{2n+1}^{2m} G_{2n} Z_{2n-2m} \tag{14}$$

$$Z_{2n+2} = \varepsilon_1 \sum_{k=0}^{n} Z_{2n-2k} \sum_{m=0}^{k} C_{2k}^{2m} X_{2m} X_{2k-2m} \tag{15}$$

$$X_{2n+2} = G_{2n+2} + \varepsilon_2 \sum_{l=0}^{n} G_{2n-2l} \sum_{k=0}^{l} X_{2l-2k} \sum_{m=0}^{k} C_{2k}^{2m} Z_{2m} X_{2k-2m} \tag{16}$$

$$C_n^k = \frac{n!}{k!(n-k)!}.$$

Thus, we may deduce from the system (5)–(7) and expansion (11)–(13) that the TCFs of interest have the nearest singularity on the imaginary axis. Retaining in the vicinity of a singularity ($|t - \mathrm{i}\tau_0| \ll |t|$) the most divergent part [22], we get

$$F^{(k)}(t) \simeq a_k/\mathrm{i}^{m_k}(\tau - \tau_0)^{m_k} \qquad k = 1, 2, 3. \tag{17}$$

Here $F^k(t)$ are $\Gamma_A(t)$, $G_0(t)$ and $\Gamma_A^z(t)$, respectively. By substitution of these equations into the system (5)–(7), initially differentiating with respect to time after rather simple algebra dealing with the selection of the most divergent terms on both sides of equations and subsequent equating of the power indices and coefficients, we obtain the indices $m_1 = m_2 = m_3 = 2$ and the functions

$$\Gamma_A(t) = -\sqrt{12/\varepsilon_1}/(t - \mathrm{i}\tau_0)^2 = -2\sqrt{6}/(t - \mathrm{i}\tau_0)^2 \tag{18}$$

$$G_0(t) \simeq -(\sqrt{12/\varepsilon_1})(1 - \varepsilon_2)/(t - \mathrm{i}\tau_0)^2 = -1.5\sqrt{6}/(t - \mathrm{i}\tau_0)^2 \tag{19}$$

$$\Gamma_A^z(t) = 2/(t - \mathrm{i}\tau_0)^2 \tag{20}$$

which are the major part of the solution of the system (5)–(7) in the vicinity of a singularity

nearest to the real axis. So, from equations (18)–(20) we may determine the distant Fourier transforms of these functions by shifting the integration contour according to the general rules [21]

$$g_k(\omega) = \Phi\{F^{(k)}(t)\} \simeq b_k |\omega| \exp(-\tau_0 |\omega|)$$
$$b_1 = 2\sqrt{6} \qquad b_2 = 1.5\sqrt{6} \qquad b_3 = 2. \tag{21}$$

Let us outline the procedure of determination of the parameter through the moments:

$$M_{2n}^{(k)} = \int_{-\infty}^{\infty} \omega^{2n} g_k(\omega)\, \mathrm{d}\omega. \tag{22}$$

Here M_{2n} are X_{2n}, G_{2n} and Z_{2n}, respectively. Since the integral function contains the term ω^{2n}, the value of the moment at large n will depend on the distant Fourier transforms of equations (21). Substituting (21) in (24), we find that

$$M_{2n}^{(k)} = d_k(2n+1)!/\tau_0^{2n+2}$$
$$d_1 = 4\sqrt{6} \qquad d_2 = 3\sqrt{6} \qquad d_3 = 4. \tag{23}$$

On the other hand, the moments determined by equation (23) enter as coefficients of expansion in the respective TCFs in a power series with respect to time (equations (11)–(13)) and they can be determined by the recurrence relations (14)–(16) obtained from the system (5)–(7).

4. Discussion and comparison with the experimental data

The recurrent relationships were used to compute the moments up to the 34th order using a computer, and subsequent determination of the $\tau_0^{(2n)}$-values were possible:

$$(\tau_x^{(2n)})^2 = 2n(2n+1)X_{2n-2}/X_{2n} \qquad (\tau_z^{(2n)})^2 = 2n(2n+1)Z_{2n-2}/Z_{2n}$$
$$(\tau_g^{(2n)})^2 = 2n(2n+1)G_{2n-2}/G_{2n}. \tag{24}$$

The results obtained are given in figure 1 as a dependence of $(\tau_0^{(2n)})^2$ on $1/n$. In agreement with the above assumptions the resultant sequence converges to a certain limiting value, 6.48, which is common to all three functions. We should emphasize that, in fact, equations (24) are expressions to determine the radius of convergence of power series (11)–(13) according to D'Alamber's criterion which is somewhat modified owing to the type of singularity (a pole of the second order). A 'direct use' of D'Alamber's criterion has as a result that equation (13*a*) ensures slow convergence. Let us evaluate the results of several sequential simplifications of the system (5)–(8). If $\Gamma_A^z(t)$ is replaced by $G_0^2(t)$

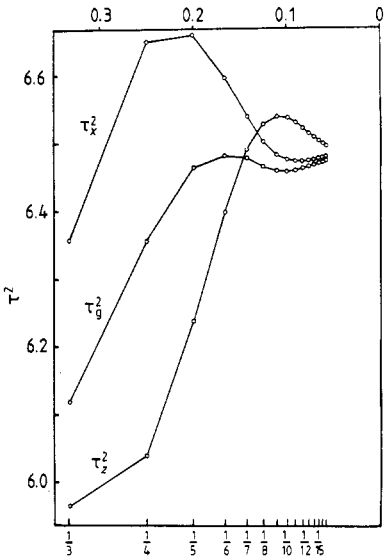

Figure 1. A position of singularity of the solution of system (11)–(13) as a function of the inverse moment number used in calculation. τ_x, τ_z and τ_g characterize the singularity of each of the above three equations.

in equation (6) in the integral function, a new system of integral non-linear equations can be constructed:

$$G_0(t) = \exp\left(-\int_0^t \int_0^{t'} \mathrm{d}t'\,\mathrm{d}t''\,\Gamma_A^z(t'')\right)$$
$$\Gamma_A^z(t) = 1 - \varepsilon_2 \int_0^t \int_0^{t'} G_0^2(t'-t'')\Gamma_A^z(t'')\,\mathrm{d}t'\,\mathrm{d}t''. \tag{25}$$

Recurrence relations for moments may now be written in the following way:

$$Z_{2n+2} = \varepsilon_1 \sum_{k=0}^{n} Z_{2n-2k} \sum_{m=0}^{k} C_{lk}^{2m} X_{2k-2m}$$
$$X_{2n+2} = \sum_{m=0}^{n} C_{2k+1}^{2m} X_{2m} Z_{2n-2m}. \tag{26}$$

The sequence of values τ_{0x}^{2n}, τ_{0z}^{2n} calculated according to equation (24) as a function of $1/n$ converges to the value $\tau_0^2 = 6.81$. In the vicinity of a singularity we obtain for the major part of solution of the system (25)

$$\Gamma_A^z(t) \simeq -2/(t - \mathrm{i}\tau_0)^2 \qquad G_0(t) \simeq -\sqrt{24}/(t - \mathrm{i}\tau_0)^2. \tag{27}$$

Thus, in spite of the above simplification the singularity remains as a pole of the second order, although its position is somewhat shifted. This procedure also results in a slight variation in coefficients.

Let us linearize the system (25) by changing $G_0^2(t)$ by $\exp(-t^2)$. Then the frequency asymptotics may be obtained by a saddle-point method [9]:

$$g(\omega) = [1/\sqrt{4\pi\omega \ln^{1/2}(16\omega)}] \exp[-\omega \ln^{1/2}(16\omega)]. \tag{28}$$

Linearization involves the elimination of the singularity (it has been shifted to a point in

Table 1. The decay constants of the exponential SDF and absorption at wings corresponding to CaF_2. The data on the shape of lines were obtained via Fourier transform of the trial function approximating experimental points [10].

Orientation	Experimental shape of lines (μs) [10]	SDF (μs)		Theory (μs)
		Experimental data [1]	Memory function method [7]	
100	49.69 ± 0.84	—	45	42.1
110	115 ± 4	57 ± 0.5	61	57
111	105.9 ± 1.6	80 ± 1	81	101

the infinite distance), since the Gauss function belongs to a class of integer functions. The linearization also resulted in a slight alteration in the dependence of the asymptotics of frequency. Nevertheless, the above approximation to a certain extent can be considered as satisfactory, since $\ln^{1/2}(\omega)$ is a slowly varying function which causes (28) to be slightly different from a pure exponential if we are interested in a not too distant wing.

At the same time, equation (28) is incorrect principally since it possesses a singularity at an infinite point in contrast to the singularity at a finite distance appearing in real systems. A condition that the determination of the above singularity involves the use of approximate system (5)–(7) does not play a significant role here. However, one can deduce from the above arguments that the non-linearity of the system (5)–(7) is of major importance in the elimination of the logarithm in a power index in (28).

The most rough operation will be the substitution of $\Gamma_A^z(t)$ for 1 in the exponential index of the first equation of the system (25). We have

$$G_0(t) = \exp(-t^2/2) \tag{29}$$

which involves unreal Gaussian frequency asymptotics [8] instead of a simple exponential.

Since the spectral asymptotics $G_0(t)$, $\Gamma_A(t)$ and $\Gamma_A^z(t)$ have been determined, the whole NMR line profile at wings can be calculated. Let us substitute (18)–(20) in equation (8). Omitting unimportant terms, we find that

$$\Gamma(t) \simeq -1.5\sqrt{6}/(t - i\tau_0)^2 - \varepsilon_3 2\sqrt{24}/6(t - i\tau_0)^2 = -14\sqrt{6}/(t - i\tau_0)^2 \tag{30}$$

and

$$g(\omega) \simeq (14/\sqrt{6})|\omega| \exp(-\tau_0|\omega|).$$

The results obtained for high-frequency asymptotics establish a direct relationship between the SDF and the shape of the wing absorption contour. Both these values should have an exponential dependence on frequency with the same index $\tau_0 \simeq 6.48/M_{2z}^{1/2}$. The computation results and respective experimental data are given in table 1. The experimental results on the shapes of lines given in the table have been obtained by the present authors using analytical calculations of the Fourier transform of the trial function used in [10] to approximate the experimental FID observed over an interval from fractions to hundreds of microseconds (i.e. at an interval $10T_2$). An exponential shape was in fact observed for the wing. The decay time (value of τ_0) is given in table 1. Experimental data on the SDF has been taken from [1]. Also, the values of SDF decay obtained by fitting

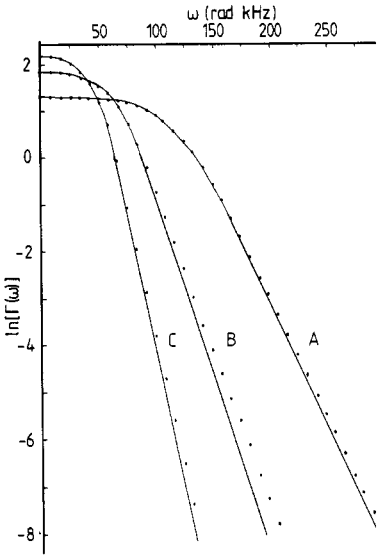

Figure 2. Logarithm of NMR absorption spectrum in single-crystal CaF_2 as a function of frequency for the field $\boldsymbol{H}_0 \| [100]$ (curve A), $\boldsymbol{H}_0 \| [110]$ (curve B) and $\boldsymbol{H}_0 \| [111]$ (curve C): ——, theory; ●, experimental data [10].

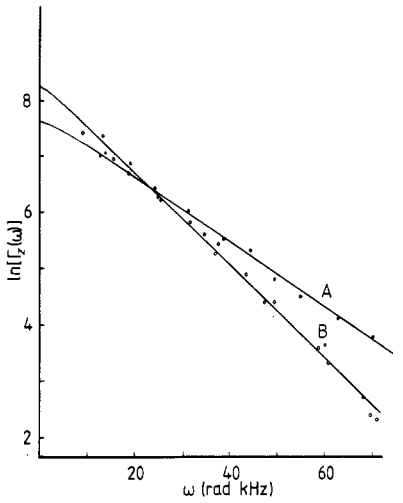

Figure 3. Logarithm of the spectrum of the Fourier function $g_z(\omega)$ versus frequency for the field $\boldsymbol{H}_0 \| [110]$ (curve A) and $\boldsymbol{H}_0 \| [111]$ (curve B): ——, theory; ●, ○, experimental data [1].

within the framework of the memory function method [7] are given in table 1. The fact that some discrepancy is obtained between the values of τ_0 determined according to the FID and SDF indicates that the real asymptotics for SDF given in [1] have not yet been attained (see figure 3). A logarithmic function of the shape of the absorption line plotted versus frequency is given in figure 2. The experimental results were obtained via transformation of Fourier arrays of experimental points taken from [10] and extended by a trial function [10] to 350 μs. The relative uncertainty in determination of a spectrum $g(\omega)$ related to the use of numerical methods (restricted time interval of definition of the function and numerical integration) was about 1%. The experimental error in [10] was 1%. The theoretical curve reflects the result of numerical solution of the system (5)–(8). The solution was obtained by the iteration technique using a computer. The function

$$G_0^0(t) \exp\left[-(B^2/2) \int_0^t (t-\tau)k(\tau)\, \mathrm{d}\tau\right]$$

was used as a first ('primer') function during solutions of this equation. The iteration was continued until

$$\max[|\Gamma_i(t) - \Gamma_{i-1}(t)|] \geqslant 0.05$$

where $\Gamma_i(t), \Gamma(t)_{i-1}$ are solutions at the ith and $(i-1)$th steps, respectively. As the above figure illustrates, good agreement between the theory and experiment was obtained. Figure 3 shows a logarithm of the Fourier transform of the function $\Gamma_A^z(t)$ plotted versus frequency. The experimental data were taken from [1]. The theoretical results were obtained in the same way as the $g(\omega)$ curves. Comparison of figures 2 and 3 indicates that the authors of [1] did not find the 'true' wing of the SDF which is presumably caused

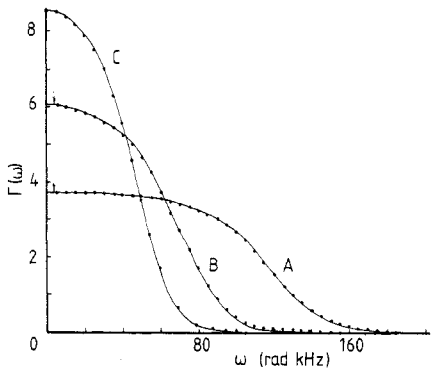

Figure 4. The spectrum of ^{19}F nuclear absorption in single-crystal CaF_2 for the field $\boldsymbol{H}_0 \| [100]$ (curve A), $\boldsymbol{H}_0 \| [110]$ (curve B) and $\boldsymbol{H}_0 \| [111]$ (curve C): ——, theory; ●, experimental data [10].

by a relatively small gyromagnetic ratio of the isotope ^{43}Ca. Figure 4 outlines the profile of the NMR line as a function of frequency. It was obtained by solving the system (5)–(8) by the above technique. An arrow indicates the frequency corresponding to the last experimental point taken in [10]. The first experimental point obtained in [10] corresponds to the approximate frequency 12.56×10^3 kHz rad.

5. Conclusion

The equations of dynamics of a nuclear spin system in solids were obtained by a rigorous method and solutions were analysed. Some remarkable experimental results [1] were explained and new predictions were made. It was stated that the wings of NMR absorption in solids were exponentials with the same decrement as the SDF. To confirm the prediction the most valuable experimental results [10] were re-examined and satisfactory coincidence of the theoretical predictions and experimental results was demonstrated.

Thus, the obtained equation enables one to account for the variety of experimental results correctly.

Acknowledgments

The authors are grateful to V A Atsarkin for his constant stimulating interest in this work and fruitful discussions and to F S Dzheparov, M A Kozhushner and T N Khazanovich for useful comments. The authors also thank P B Medvedeva for instructive discussions of the mathematical procedures involved.

Appendix

The coefficients of expansions of the TCF into a time power series (moments) can be expressed through multiple commutators with a Hamiltonian. For instance, for TCF $\Gamma_A(t)$,

$$X_{2n}^A = \mathrm{Sp}\{[H, H, \ldots, [H, S_i^+] \ldots] S_i^-\} / \mathrm{Sp}(S_i^+ S_i^-) \tag{A1}$$

while using a diagram technique [14] a process of computation of commutators in moments (A1) should be considered at the first stage.

Each act of commutation with an additive H_{zz} from (1) is related to the 'longitudinal vertex' (corresponding to the b_{ij})

(A2)

and commutation with an additive H_{ff} from (1) to a transverse vertex (corresponding to an index a_{ij})

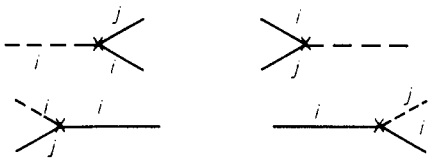

(A3)

The operator S_z is designated by a broken line, whereas the operators S^+ or S^- are designated by a full line marked with an arrow if necessary and directed in an opposite manner depending on the type of operator.

The moment M_{2n} corresponds to the sum of all possible diagrams containing $2n$ vertices, and the number of lines increases when passing through n vertices, whereas the rest of vertices (n) decreases the number of lines when the diagram passes along the time axis (from the left to the right in equations (A2) and (A3)).

Thus, every diagram begins and ends by one line corresponding to operators S_i^α or S_j^α ($\alpha = Z, +, -$) depending on the type of correlation function. All vertices should be connected between each other by at least one line (according to the theorem of connection [14]). As an example let us show all diagrams giving an input into the second moments.

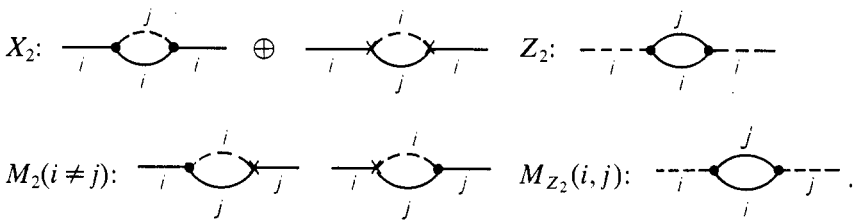

(A4)

A summation is realized over all the inner indices i, j, present in the diagrams. Each diagram is multiplied by a time factor obtained after distribution of time variables t_1, $t_2, \ldots, t_{2n}$ at vertices from the left to the right and computation of the integral

$$\int_0^t \mathrm{d}t_1 \int_0^{t_1} \mathrm{d}t_2 \ldots \int_0^{t_{2n-1}} \mathrm{d}t_{2n}.$$

The obtained diagrams can be divided into reducible and irreducible. As usual, the diagrams are called reducible if we can decompose them in two parts by cutting along one line. The summation of diagram series is realized [14] by replacement of all thin lines by thick lines upon an irreducible diagram. Each thick line is then related to a proper correlation function ($\Gamma_A(t)$, $\Gamma_A^z(t)$). Although an input of cross TCF can be taken into account during summation it is negligibly small for high Z [18, 21]. The above procedure is precise when $Z \to \infty$ [14].

Thus, the memory functions in equations (3) and (4) are the series with respect to irreducible diagrams with increasing number of vertices:

$$R^{\alpha}(t) = \sum_{m=1}^{\infty} R^{\alpha(2m)}(t). \tag{A5}$$

The index α in (A5) distinguishes between irreducible operators for TCFs $\Gamma_A^z(t)$ and $\Gamma_A(t)$.

The first terms in expansion (A5) are obtained from irreducible parts of the skeleton diagrams (A4) via replacement of thin lines by thick lines. Consequently,

$$R_A^{(2)}(t) = \varepsilon_3 \Gamma_A(t)\Gamma_A^z(t) \tag{A6}$$

$$R^{z(2)}(t) = \varepsilon_1 \Gamma_A^2(t) \tag{A7}$$

$$R^{(2)}(t) = \varepsilon_4 \Gamma_A(t)\Gamma_A^z(t) \tag{A7a}$$

$$\varepsilon_4 = 9/4$$

the mth term of the series being a sum of integrals of production of autocorrelation functions. We show all the diagrams of the fourth order for $R^{(4)}(t)$ as an example:

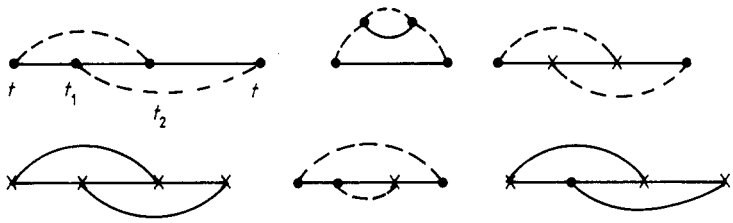

and apparent expressions for their input [15]

$$\begin{aligned} R^{(4)}(t) = &-\left(\frac{9}{4} + \frac{45S_2}{16S_1^2}\right)\int_0^t dt_1 \int_0^{t_1} dt_2\, \Gamma_A(t-t_1)\Gamma_A(t_1-t_2)\Gamma_A(t_2) \\ &\times \Gamma_A^z(t-t_2)\Gamma_A^z(t_1) - \left(\frac{9}{16} - \frac{9}{16}\frac{S_2}{S_1^2}\right) \\ &\times \int_0^t dt_1 \int_0^{t_1} dt_2 \Gamma_A^z(t-t_1)\Gamma_A(t_1-t_2)\Gamma_A^z(t_2)\Gamma_A(t-t_2)\Gamma_A(t_1) \\ &- \frac{9}{4}\frac{S_2}{S_1^2}\int_0^t dt_1 \int_0^{t_1} dt_2\, \Gamma_A(t-t_1)\Gamma_A(t_1-t_2)\Gamma_A(t_2) \\ &\times \Gamma_A^z(t)\Gamma_A^z(t_1-t_2) \\ &+ \frac{9}{8}\frac{S_2}{S_1^2}\int_0^t dt_1 \int_0^{t_1} dt_2 \Gamma_A(t)\Gamma_A^z(t-t_1)[\Gamma_A(t_1-t_2)]^2\Gamma^z(t_2) \end{aligned} \tag{A8}$$

$$S_1 = \sum_j b_{ij}^2 \qquad S_2 = \sum_{j,k} b_{ij}^2 b_{ik} b_{jk}.$$

Let us now retain only the diagrams with longitudinal vertices in a series for $\Gamma_A(t)$ conserving the transverse vertices in a process of the replacement of an ordinary broken

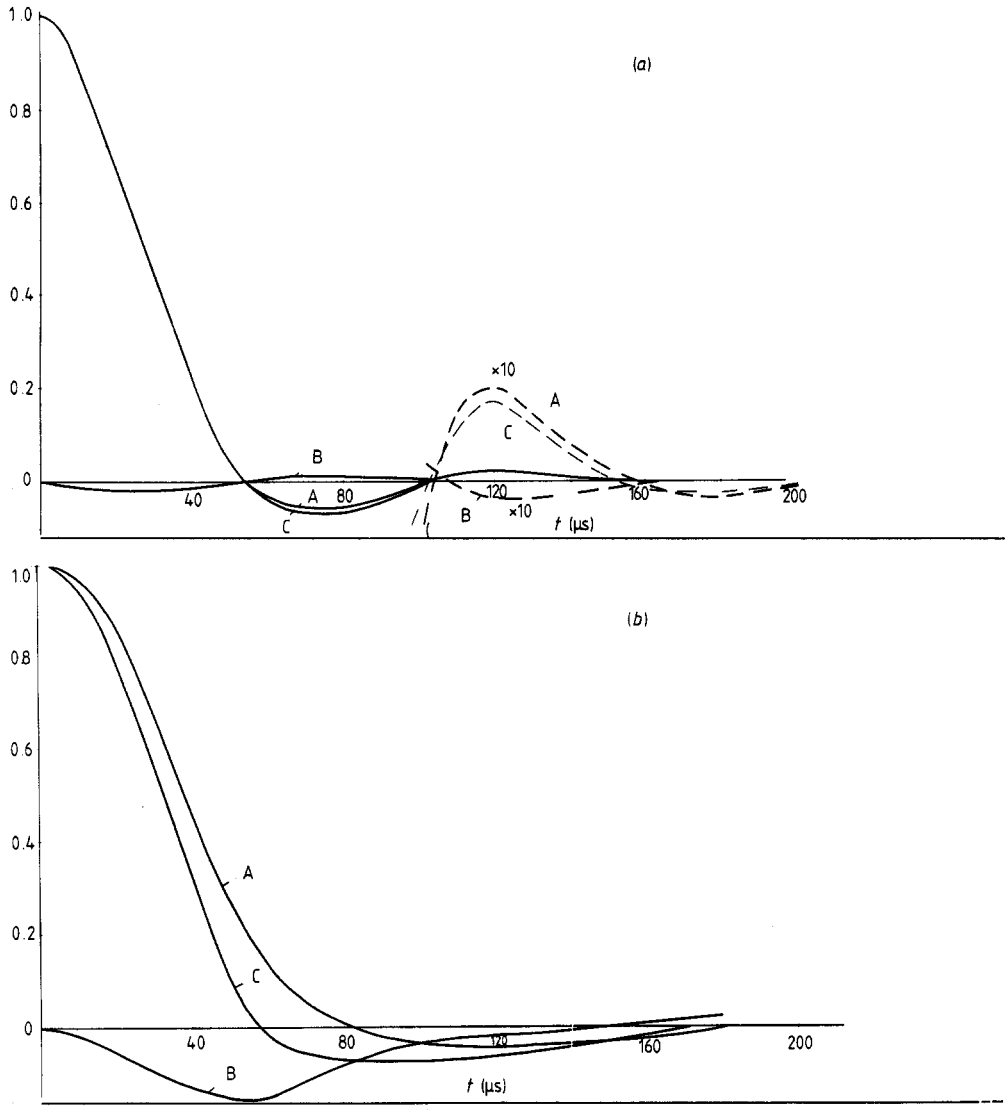

Figure A1. Corrections originating in diagrams with four vertices ($\boldsymbol{H}_0 \| [111]$): curve A, the signal of free precession without correction; curve B, corrections; curve C, the corrected signal of free precession. (*b*) The same as (*a*) plotted for the kernel (A11*a*).

line by only a thick line, i.e. during renormalization of lines corresponding to operators $\{S_i^+\}$, but we shall neglect transverse vertices when normalizing lines for $G_0(t)$. Designating the sum of interest of a diagram series as $G_0(t)$ and the corresponding irreducible operator (memory function) as $Q(t)$, we obtain

$$\frac{\mathrm{d}G_0(t)}{\mathrm{d}t} = -\int_0^t Q(t-t_1)G_0(t_1)\,\mathrm{d}t_1. \tag{A9}$$

The first two diagrams for $Q(t)$ can be plotted as follows:

(A10)

(the wavy line denotes the function $G_0(t)$) and the corresponding apparent expression is

$$Q_2(t) = G_0(t)\Gamma_A^z(t)$$
$$Q^{(4)}(t) = -\int_0^t \int_0^{t_1} dt_1\, dt_2\, G_0(t-t_1)G_0(t_1-t_2)G_0(t_2)\Gamma_A^z(t_1-t_2)\Gamma_A^z(t_1). \tag{A11}$$

Thus, $G_0(t)$ is the autocorrelation function of the transverse component of a spin in a local z field, modulated by flip-flop interaction, i.e. FID for the Anderson model [10, 11]. The above diagram series for $G_0(t)$ can be summed directly [17] without use of the irreducible operator because all longitudinal vertices corresponding to the rotation around a fixed axis z are commutative and, consequently, the numerical coefficient in front of the diagram depends on the number of vertices and does not depend on their distribution along the time axis.

The summation yields

$$G_0(t) = \exp\left(-\int_0^t \int_0^{t_1} \Gamma_A^z(t_2)\, dt_2\right) \tag{A12}$$

i.e. the ordinary Anderson function [10]. The result obtained corresponds to the lowest approximation in the cumulant expansion; because the permutability of vertexes corresponds to turns about the same axis (in our case z), all higher cumulants become 0.

The results of calculation of corrections originating in all diagrams with four vertices are given in figure A1:

$$R^{(2)}(t) + R^{(4)}(t) - Q^{(2)}(t) - Q^{(4)}(t) = [R(t) - Q(t)]^{(4)}. \tag{A11a}$$

These figures also show the time dependence of the irreducible operator containing two and four vertex inputs. As these figures indicate, the correction due to $R^{(4)}(t)$ is small.

References

[1] McArthur D A, Hahn E L and Walstedt R E 1969 *Phys. Rev.* B **188** 609
[2] Stokes H T and Alion D C 1977 *Phys. Rev.* B **15** 1271
[3] Garroway A N 1979 *J. Magn. Reson.* **34** 283
[4] Safin V A, Skrebnev V A and Vinokurov V M 1984 *Zh. Exp. Teor. Fiz.* **87** 1889 (in Russian)
[5] Abragam A and Gol'dman M 1982 *Nuclear Magnetism: Order and Disorder* (Oxford: Clarendon) ch 1
[6] Forster D 1975 *Hydrodynamic Fluctuations, Broken Symmetry and Correlation Functions* (New York: W A Benjamin) ch 1
[7] Demco D E, Tegenfeldt J and Waugh J S 1975 *Phys. Rev.* B **11** 4133
[8] Danner V and Vagner M 1984 *J. Chem. Phys.* **81** 5054
[9] Zobov V E and Lundin A A 1986 *Zh. Exp. Teor. Fiz. Pis. Red.* **43** 418 (in Russian)
[10] Engelsberg M and Low I J 1974 *Phys. Rev.* B **10** 822
[11] Abragam A 1961 *The Principles of Nuclear Magnetism* (Oxford: Clarendon) ch 4
[12] Berne B J and Harp G D 1970 *Adv. Chem. Phys.* **17** 63–227
[13] Lado F, Memory J D and Parker G W 1971 *Phys. Rev.* B **4** 1406
[14] Resibois P and De Leener M 1966 *Phys. Rev.* **122** 305, 318
[15] Borckmans P and Walgraef D 1967 *Physica* **80** 35; 1973 *Phys. Rev.* B **7** 563

[16] Winter J M 1971 *Ann. Phys., NY* **6** 167
[17] Zobov V E, Lundin A A and Makarenko A V 1987 *LV Kirensky Institute of Physics, Siberian Branch of the Academy of Sciences of the USSR, Krasnoyarsk, Preprint* 436 F (in Russian)
[18] Jensen S J K and Hansen K E 1976 *Phys. Rev.* B **13** 1903
[19] Lundin A A and Provotorov B N 1976 *Zh. Exp. Teor. Fiz.* **70** 22a (in Russian)
[20] Lundin A A and Makarenko A V 1984 *Zh. Exp. Teor. Fiz.* **87** 999 (in Russian)
[21] Migdal A B 1975 *Kachestvennye Metody v Kvantovoi Teorii (Qualitative Methods in Quantum Theory)* (Moscow: Nauka) (in Russian)
[22] Golubev D V 1950 *Lektsii po Analiticheskoi Teorii Differentsial'nykh Uravnenii (Lectures on Analytical Theory of Differential Equations)* (Moscow: Gostekhizdat) (in Russian)